EIGHTEENTH EUROPEAN ROTORCRAFT FORUM

A - 02

Paper N°17

COMPUTATION OF THE LOADS ON THE AH-1/OLS MODEL ROTOR IN FORWARD FLIGHT AND COMPARISON WITH WIND TUNNEL TESTS

M. SCHAFFAR, J. HAERTIG
ISL,FRANCE

September 15-18, 1992

AVIGNON, FRANCE

ASSOCIATION AERONAUTIQUE ET ASTRONAUTIQUE DE FRANCE

COMPUTATION OF THE LOADS ON THE AH-1/OLS MODEL ROTOR IN FORWARD FLIGHT AND COMPARISON WITH WIND TUNNEL TESTS

M. SCHAFFAR, J. HAERTIG

French-German Research Institute
5 rue du Général Cassagnou
68301 SAINT-LOUIS (France)

Abstract

The vortex lattice method jointly used with a local conformal mapping (to transform the thin blade into a thick one) is briefly described. In order to validate the aerodynamic code, the results are compared with wind tunnel tests for one flight case of the AH-1/OLS model rotor.
The study of the wake shows 4 blade/wake interactions for blade 1 during one revolution but only two parallel interactions occur in the rotor plane; the comparison of the computed and measured blade pressures shows an over-estimation on the advancing side and an acceptable agreement on the retreating side.

Notation

c	chord length
C_p	pressure coefficient
C_T	thrust coefficient
(i,j)	index, chordwise and spanwise
l	(subscript) lower side of the blade
N	total panel number
N_X,N_Y	panel number chordwise and spanwise
R	rotor radius
u	(subscript) upper side of the blade
U_∞,U_x	velocity of the ambient air
x,y,z	coordinate system
β_j^k	circulation shed in the wake
Γ,$\Gamma_{i,j}$,$\gamma_{i,j}$	panel bounded circulation
μ	advancing coefficient
φ	perturbation potential
ψ	azimuth angle in the rotor plane
θ	pitch angle
θ_c,θ_s	cyclic pitch
Ω	angular rotational velocity

1.Introduction

Rotor blade/vortex interaction (BVI) noise is one among several noise sources for helicopters during low speed or landing flight, when the blade/wake interactions occur. A lot of theoretical and experimental work has been achieved in the last years to study this phenomenon.

Before computing the noise, it is necessary to know the loads acting upon the blades. Since three years we have developed an aerodynamic code named ROTAR, in order to compute the loads on the rotor blades [1,2,3,4] which serve as input data for an acoustic code named ROTAC (presented in Paper 15,"Validation of the ROTAC code for the rotor noise prediction", P.Gnemmi, J.Haertig, Ch.Johé).

Nevertheless, a direct comparison of the aerodynamic results with measured results on rotor blades has not been made. In cooperation with the ONERA it was decided to validate the aerodynamic code by a confrontation with wind tunnel tests achieved by the DLR and the US Army in the DNW wind tunnel in 1982 on the AH-1/OLS model rotor [5,6]; the measured data were obtained from the ONERA.

In this paper we present an application of our method (based on the Vortex Lattice Method) to one flight test of the AH-1/OLS model rotor. In the following sections, we will briefly describe the Vortex Lattice Method (VLM) and the method used to thicken the blade. Finally the results obtained

for the AH-1/OLS model rotor in advancing flight will be presented.

2.Description of the computational method (ROTAR Code)

Description of the VLM

Using Green's theorem, the solution of the Laplace equation for the perturbation potential φ leads to a sources and doublets distribution on the blades and doublets on the wake; for thin blades only the doublets distribution is necessary; in our case, for each panel, we use the equivalence between a constant surface doublet and peripherical vortex lines.

Each of the two blades is divided into $N = N_x \cdot N_y$ quadrilateral panels (N_x chordwise, N_y spanwise,see figure 1). On this panel system, we map a bound vortex lattice with vortex lines of the strength $\Gamma^n_{i,j}$ in the spanwise direction (figure 1) and vortex lines in the chordwise direction whose strength $\gamma^n_{i,j}$ is defined by:

$$\gamma^n_{i,j} = \sum_{k=1}^{i} \left(\Gamma^n_{k,j-1} - \Gamma^n_{k,j}\right) \qquad (1)$$

where n indicates the time step.

At each time step the conservation of the circulation is warranted by the shedding of an unsteady vortex line β^n.

The wake lattice is built stepwise with the vortices $\beta_j{}^{k'}$ and $\gamma_j{}^{k'}$ (previously shed) whose circulation remains constant.

The non-penetration condition gives a system of N linear equations by writing the induced velocities at each control point using the Biot-Savart law . In this law we have a source of numerical problems if the distance between the vortex segment and the control point is too small. We need a regularization which has to be chosen carefully in order to simulate the growing of a vortex core.

We use a regularization length which increases linearly with its age, following an experimental law found in the literature [7].

The pressure jump across the blades $\Delta p_{i,j} = -(p_l - p_u)_{i,j}$ is obtained with the Bernoulli equation written for the upper (u) and the lower (l) side of the blade:

$$-\left(\frac{p_l - p_u}{\rho}\right)_{i,j} = \left[-\frac{\partial(\varphi_u - \varphi_l)}{\partial t} + \frac{U_l^2 - U_u^2}{2}\right]_{i,j} \qquad (2)$$

At the end of the time step n, the normalized rotor thrust coefficient C_T is computed.

The computational step is varied during the calculation: one and a half revolution is made with a 10° step, then the step is decreased until 5°; if a better precision is needed (for the noise prediction, for example,) the step can be reduced to 1° for one half revolution with obviously a larger CPU time consumption.

Description of the method used to thicken the blade

The Vortex Lattice Method computes the loads for a thin blade. We need another method in order to obtain the loads acting upon a thick blade.

At each time step the following assumption is made: for each position in span a conformal mapping can be used to extrapolate the results to a thick blade, assuming that the potential φ remains the same. We use the Joukowski transformation for a symmetrical profile and the Theodorsen transformation for a non-symmetrical profile. The potential φ is obtained by integrating the velocity along a line coming from infinity , 10 spans in the z-direction to the inner LE (leading edge) and by adding (upper side) or by subtracting (lower side) half of the encountered singularity $\Gamma_{i,j}$ from one control point to the next.

Pressure coefficients $(C_p)_{u,l}$ are then calculated for the upper and the lower side of the *"thick" blade.*

This method has been compared with a source-doublets method applied to a thick wing with an angle of attack of 10° (see figure 2); except fo a very small area near the leading edge where our thickening method gives too large values, the two methods practically give the same results. The OLS symmetrical blade profile was approched by two types of profiles: a Joukowski profile with 9.7% thickness and a NACA0012 profile.

3.Application to the AH-1/OLS model rotor

The rotor used here is the two-bladed AH-1/OLS model rotor [5]. The rotor characteristics are the following ones:

- chord c = 0.104 m,
- radius R = 0.958 m,
- blade root distance R_0 = 0.174 m,
- linear blade twist 10°/m,
- OLS blade profile :

The flight conditions are:

- rotor inclination angle α_Q = 1°,
- coning angle = 0.°,
- flapping angles = 0.°,
- advancing coefficient μ = 0.163,
- collective pitch θ_0 = 5.31°,
- cyclic pitch θ_c = 1.86°,θ_s = -1.87°, with the following law:
  $\theta = \theta_0 + \theta_c * \cos(\psi) + \theta_s * \sin(\psi)$,
- mean thrust coefficient C_T = 0.00535,
- air velocity U_∞ = 36.72 m/s,
- temperature = 12°.

Aerodynamic results

For the aerodynamic calculations the typical parameters are: 12 panels in the chordwise direction, 14 panels in the spanwise direction, 5° as azimuthal step. These spatial definitions and the azimuthal one are sufficient for the normal aerodynamic computation, but when the loads are fed into the acoustic code ROTAC, the spatial definitions and the azimuthal one have to be refined: better results will be obtained with 18x22 panels on each blade and 1° as azimuthal step with a computation time 10 times higher; this will be confirmed in Paper No 15.

Thrust and circulation

The time evolution of the total thrust is shown in figures 3 and 4. After a starting period we find a curve with a periodical shape; figure 4 gives the thrust evolution for the last computed revolution: we can see that the two halves of the thrust curve (azimuth angle 0° to 180° and azimuth angle 180° to 360°) are practically the same. Two strong "spikes" are produced by blade/wake interactions on the advancing side (azimuth 60° for blade 1 and 240° for blade 2) and two low "spikes" are produced by retreating blade/wake interactions (azimuth angle 150° for blade 2 and 330° for blade 1). The computed mean value of the thrust is 0.0049, this is a little smaller than the measured value (0.00535); we do not have any satisfying explanation for this deviation which may be related to some uncertainty concerning the flight parameters.

The time evolution of the normalized circulation ($\Gamma^*100./\Omega R^2$) of the blade 1 tip vortex is shown on figure 6 in comparison with the evolution of the cyclic pitch at y/R = 0.70 shown on figure 5. The general behavior of these two quantities is similar: on the advancing side the vortex strength decreases with the decreasing angle of attack of the blade and on the retreating side the vortex strength increases with the increasing angle of attack of the blade. We can also see "spikes" which correspond to several blade/wake interactions.

Figure 7 depicts the distribution of the normalized circulation (Σ_i ($\Gamma_{i,j}$), see figure 1) on the rotor disk for blade 1. This contour plot presents several regions with strong circulation:

1. for the azimuth angle ψ, varying from -30 to 30°, we have the strongest "mountain" of circulation which corresponds to the maximum of the angle of attack; the minimum of the pressure on the blade will be found in this region as shown later (fig. 17);
2. for the azimuth angle ψ, varying from 210 to 285°, we find a second region with strong cir-

culation, the shape of which is very different from the first one (the contour lines being more stretched); this second region will also be found in the low pressure distribution on the blade;

3. some "spots" are also found for the azimuth angles 60° and 90° which correspond to blade/wake interactions.

Figure 8 presents the normalized circulation shed in the wake for each azimuth angle for blade 1 during one rotor revolution ($\gamma_{n,j}$, see figure 1). Here, the maximum of circulation is shed for a small region near the blade tip; negative circulation is shed near the root of the blade.

Analysis of the blade/wake interactions

With a postprocessing code the wake is analysed to obtain all blade/wake interactions for blade 1 during one rotor revolution (location, age and strength of the vortex interacting with the blade). Figure 9 shows the four interactions which occur in this case:

1. an oblique interaction on the advancing side and a near-parallel interaction on the retreating side with the wake of blade 1;
2. a parallel interaction near the azimuth angle of 45° with the wake of blade 2;
3. an oblique interaction on the advancing side with the wake of blade 1;
4. a perpendicular or oblique interaction with the wake of blade 2; this interaction sweeps on half of the rotor disk.

Figure 10 depicts the span location of the interactions. Interactions "1" and "4" only concern the external half of the blade while the other two interactions concern the whole blade.

The height (h/c) above the rotor plane (no coning and no flapping angles) is given on figure 11. Interaction "1" occurs below the rotor plane, interactions "2" and "3" near the rotor plane ($h/c = \pm 0.4c$) and thus near the blade and interaction "4" occurs above the rotor plane.

The age is expressed by the angle $\Omega\ \Delta t$, Δt being the delay between the emission of this tip vortex and the interaction. The evolution of this age is shown on figure 12: for the interactions "1" and "2" the vortex is "old" (more than 1 revolution), for interactions "3" and "4" the vortex is younger (3/4 of a revolution for interaction "3" and half of a revolution for interaction "4"). The ages are different but, as shown on figure 13, the vortex strength for all interactions lies between 0.5 and 0.7, which is much lower than the maximum value of 1.2 (see figure 6).

Comparison of the computed and measured pressures on the blades

The pressures transducers are located near the leading edge ($x/c = 0.03$ for several positions in span) and at a given span ($y/R = 0.955$). The computational control points are located at the same positions as those used in the experiment.

The comparison between the measured and computed differential pressures is given on figures 14 and 15. These figures lead to the following conclusions:

the deviations between the two tested profiles (Joukowski or Naca0012) are not very important

for $x/c = 0.03$ the computed differential pressures are generally lower than the measured ones on the advancing side and practically equal on the retreating side; this deviation disappears more or less for points behind the leading edge; these discrepancies are not clearly explained and in fact the compressibility effects which are neglegted in the computation (M_{AT} near 0.75 for the advancing blade) may change this behavior;

every blade/wake interaction measured by the pressure transducers is also found in the computation, but the slope of the measured interactions is often steeper than that of the computed ones. This may be one reason for a bad agreement in the acoustic case when the loads computed with an azimuthal step of 5° are fed into the ROTAC code.

Figures 16a,b show a contour plot of the computed (16a) and the measured pressures (16b) on the rotor disk: the two figures are very similar. One notes "pressure sinks" which correspond to the "mountains" of circulation already demonstrated on figure 8. Figures 17a,b show a contour plot of the time derivatives of the computed pressures (17a) and the measured pressures (17b) on the rotor disk: the blade/wake interactions which produce the highest derivatives are clearly visible at practically the same locations. Nevertheless, the highest computed level is roughly half of the measured one; this discrepancy may arise from the choice of the azimuthal step for this computation.

4. Concluding remarks

The numerical simulation presented in this paper seems to be a good compromise as compared with more sophisticated CFD methods for helicopter rotor computation. This method was applied to the aerodynamic computation of the AH-1/OLS model rotor tested in the DNW wind tunnel. The variation of measured and predicted pressures due to blade/vortex interactions are in phase and very similar in shape.

With a "normal" CPU time consumption with an azimuthal step of 5° all aerodynamic quantities show an acceptable agreement with the measurement.

This comparison has also shown some discrepancies between computation and measurement, especially for the mean thrust and for the pressures on the advancing side. These deviations may be related to some uncertainties (flight parameters, blade deformation, flapping, etc) changing consequently the height of the interaction. Moreover, compressibility effects (which are neglected in this computation) may explain discrepancies on the advancing blade side.

Nevertheless, when the loads are used for noise prediction, the panel number must be increased and the azimuthal step must be smaller (the computation time being obviously much higher in this case).

In the future, this method (VLM with local conformal mapping) can also be applied with some minor modifications of the ROTAR code to study the flow around a rotor with a fuselage.

BIBLIOGRAPHY

1. M.Schaffar, J.Haertig and P.Gnemmi, Aerodynamic loads and blade/vortex interaction noise prediction, 15th European Rotorcraft Forum, Paper 3, Amsterdam, Netherlands, 12-15 Sept. 1989
2. M. Schaffar, J. Haertig and P. Gnemmi, Computation of the BVI noise for the BO105 model rotor in forward flight and comparison with wind tunnel tests, 47th AHS Forum, Phoenix, Arizona, USA, 5-7 May 1991
3. J. Haertig and P. Gnemmi, Calcul du bruit d'épaisseur et du bruit de charge rayonnés par un rotor en vol d'avancement, ISL-Report R 119/89, Saint-Louis, France
4. M. Schaffar, J. Haertig and P. Gnemmi, Interaction pale/sillage sur un rotor bipale avec prévision du bruit rayonné (vol stationnaire et vol d'avancement, comparaison calcul/expérience), ISL-Report R 120/89
5. W.R. Splettstoesser, K.J. Schultz, D.A.Boxwell and F.H.Schmitz, Helicopter model rotor blade/vortex interaction noise: scalability and parametric variation, NASA TM 86007, Dec.1984
6. K.J. Schultz and W.R. Splettstoesser, Measured and predicted impulsive noise directivity characteristics, 13th European Rotorcraft Forum, Paper 1.2, Arles, France, Sept. 8-11, 1987
7. T.L. Thompson, O.J. Kwon, J.L. Kemnitz, N.M. Komerath and R.B.Gray, Tip vortex core measurements on a hovering rotor, AIAA Paper 87-0209, 1987

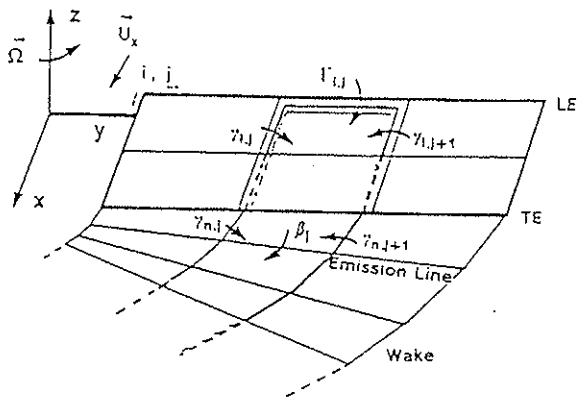

Fig. 1: Vortex Lattice on the blade and in the wake

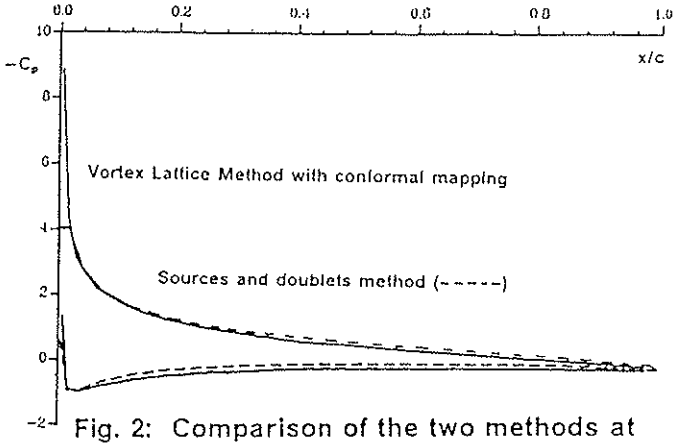

Fig. 2: Comparison of the two methods at y/R = .75 for a wing at 10° incidence

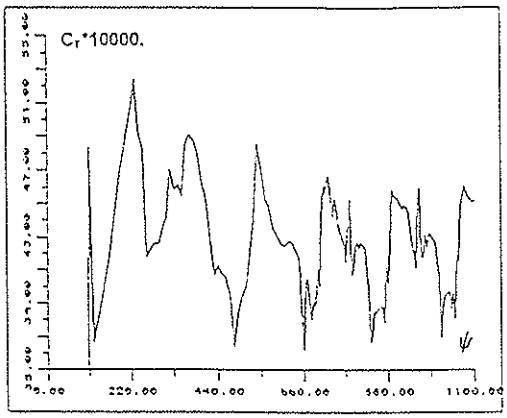

Fig. 3: Evolution of the thrust coefficient

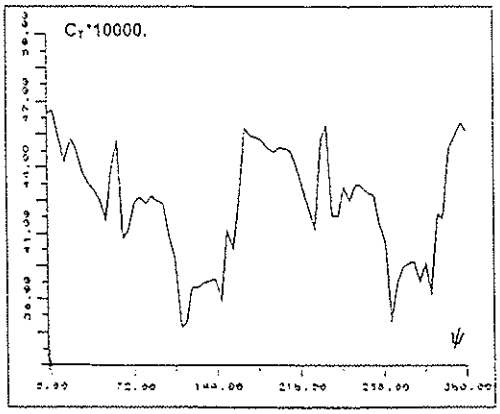

Fig. 4: Evolution of the thrust coefficient for one rotor revolution

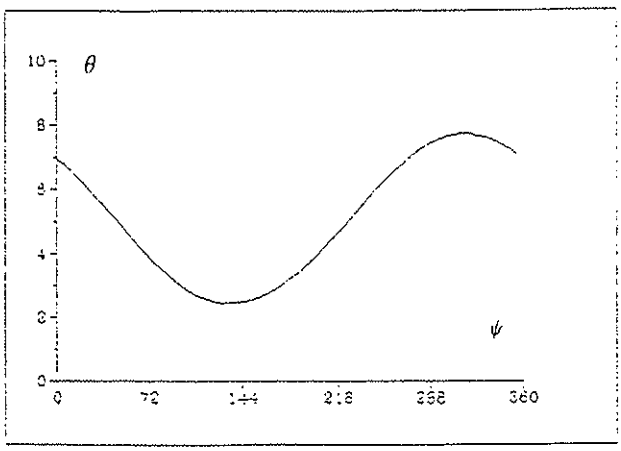

Fig. 5: Evolution of the cyclic pitch during one rotor revolution at y/R = 0.70

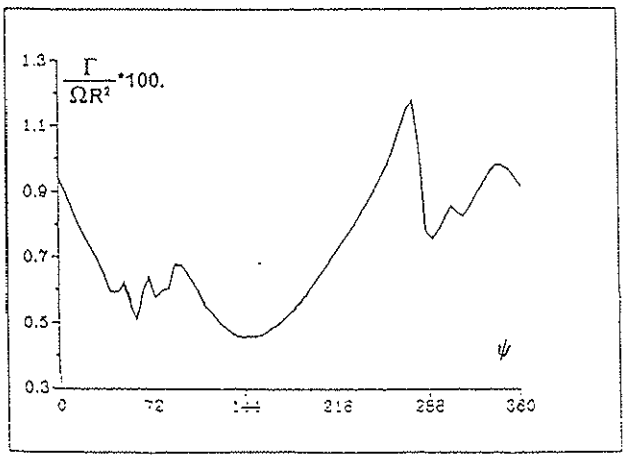

Fig. 6: Tip vortex strength for one revolution of blade 1

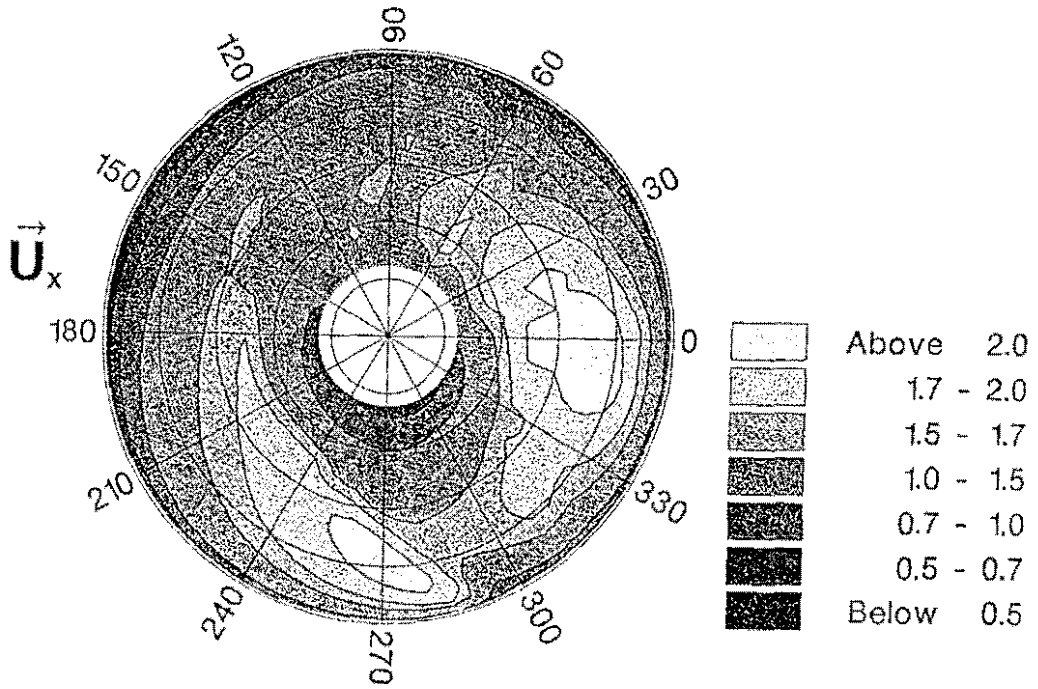

Fig. 7: Contour plot of the normalized circulation on the rotor disk for blade 1

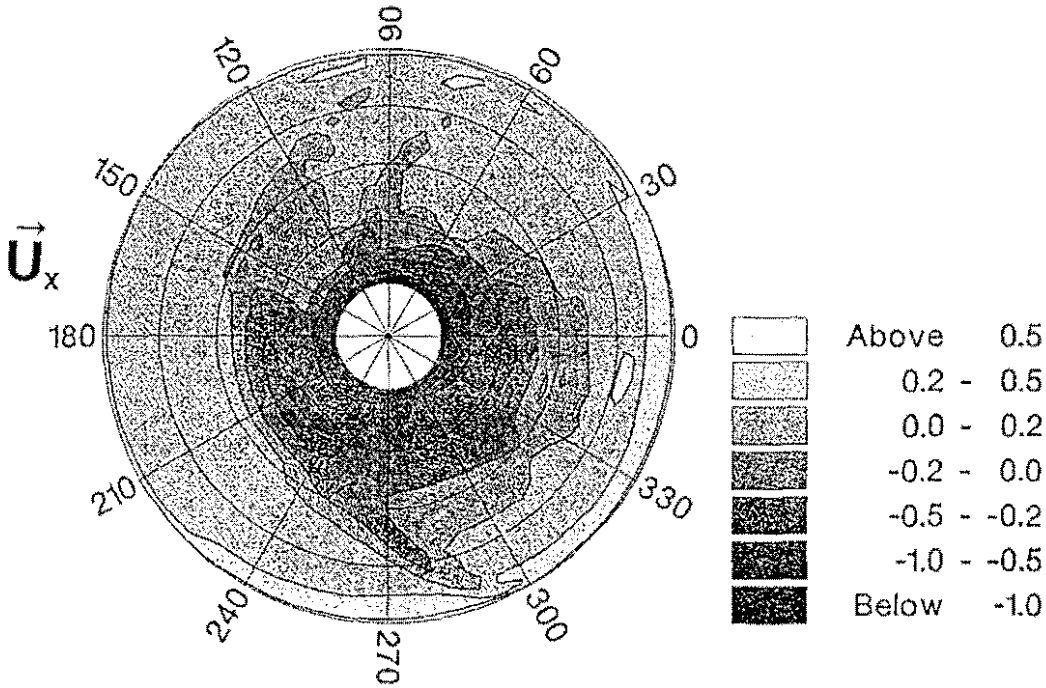

Fig. 8: Contour plot of the normalized circulation shed in the wake during one revolution of blade 1

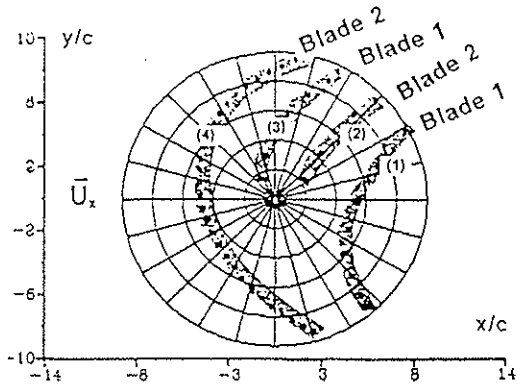

Fig. 9: Locations of the blade/wake interactions on the rotor disk

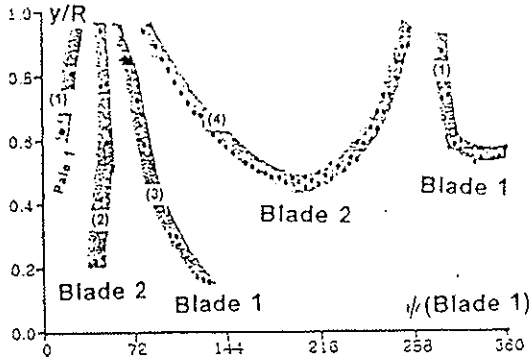

Fig. 10: Span location of the four blade/wake interactions

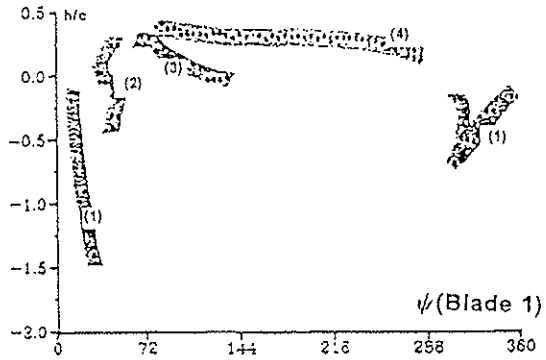

Fig. 11: Height of the four blade/wake interactions

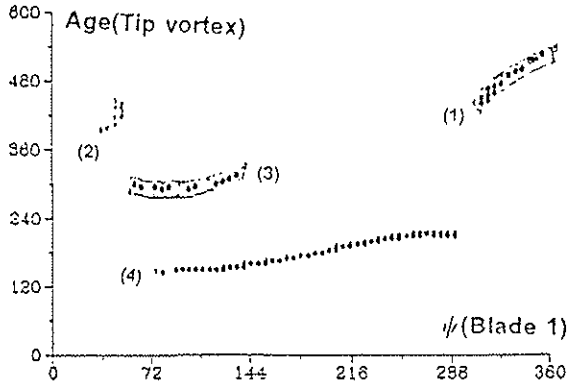

Fig. 12: Age of the tip vortex for the four interactions

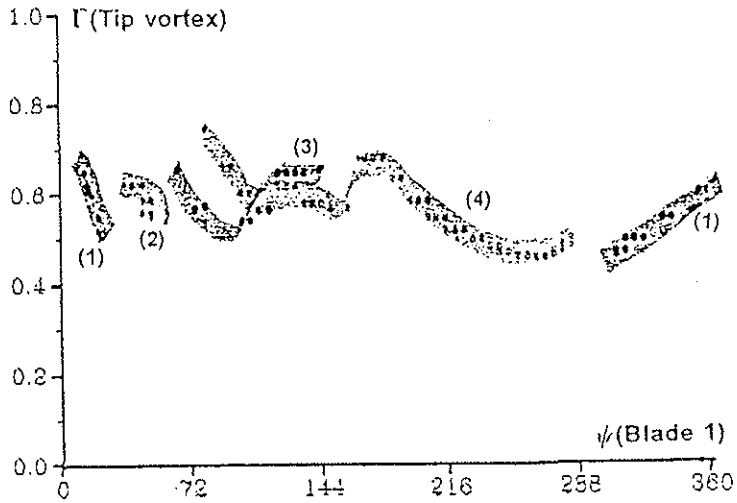

Fig. 13: Intensity of the interacting tip vortex

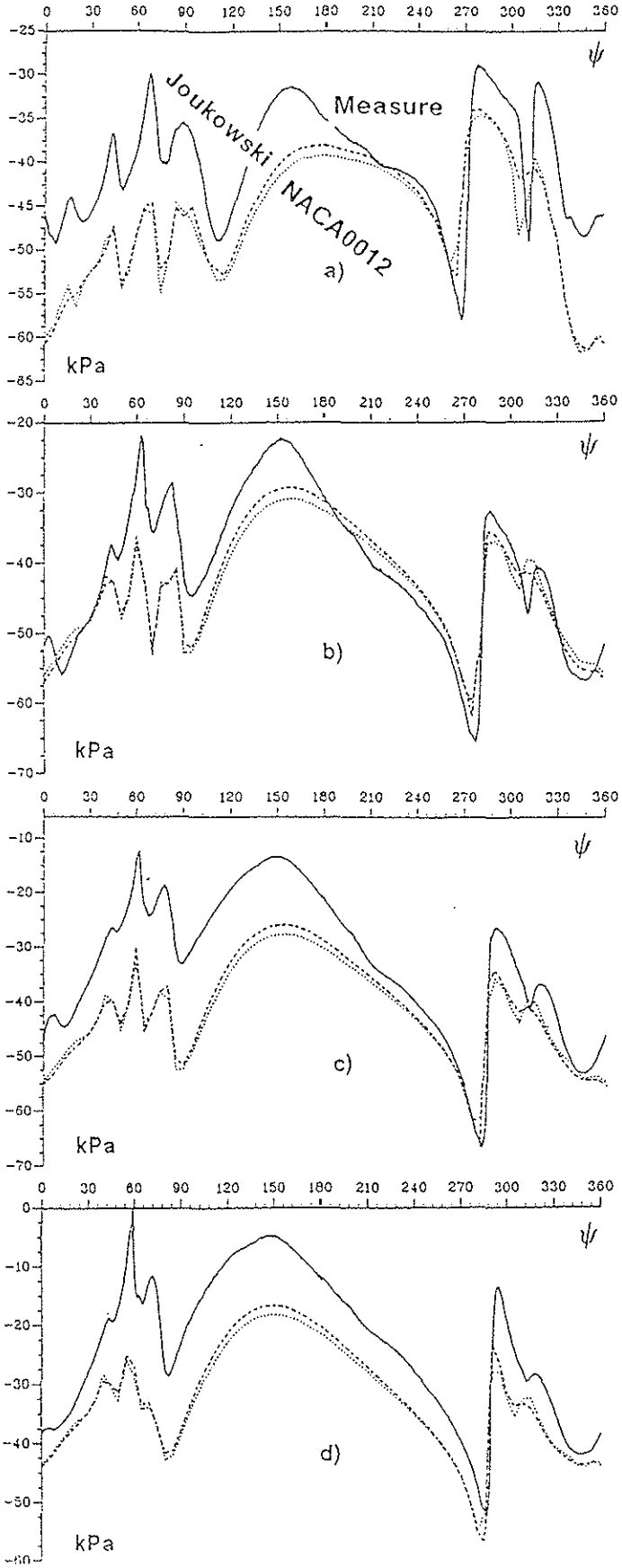

Fig. 14: Comparison of the computed and the measured differential pressures for x/c = 0.03 and : a) y/R = .75, b) y/R = .86, c) y/R = .91, d) y/R = .975

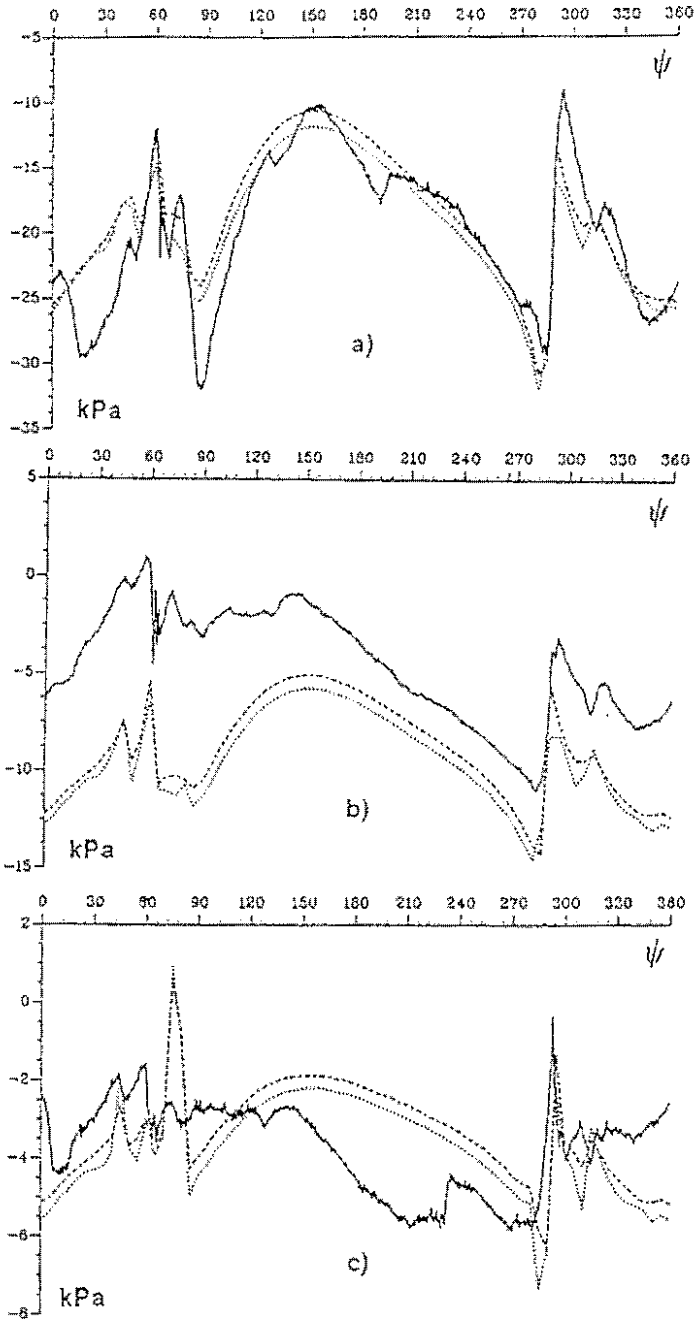

Fig. 15: Comparison of the computed and the measured differential pressures for y/R = 0.955 and : a) x/c = .08, b) x/c = .25, c) x/c = .50

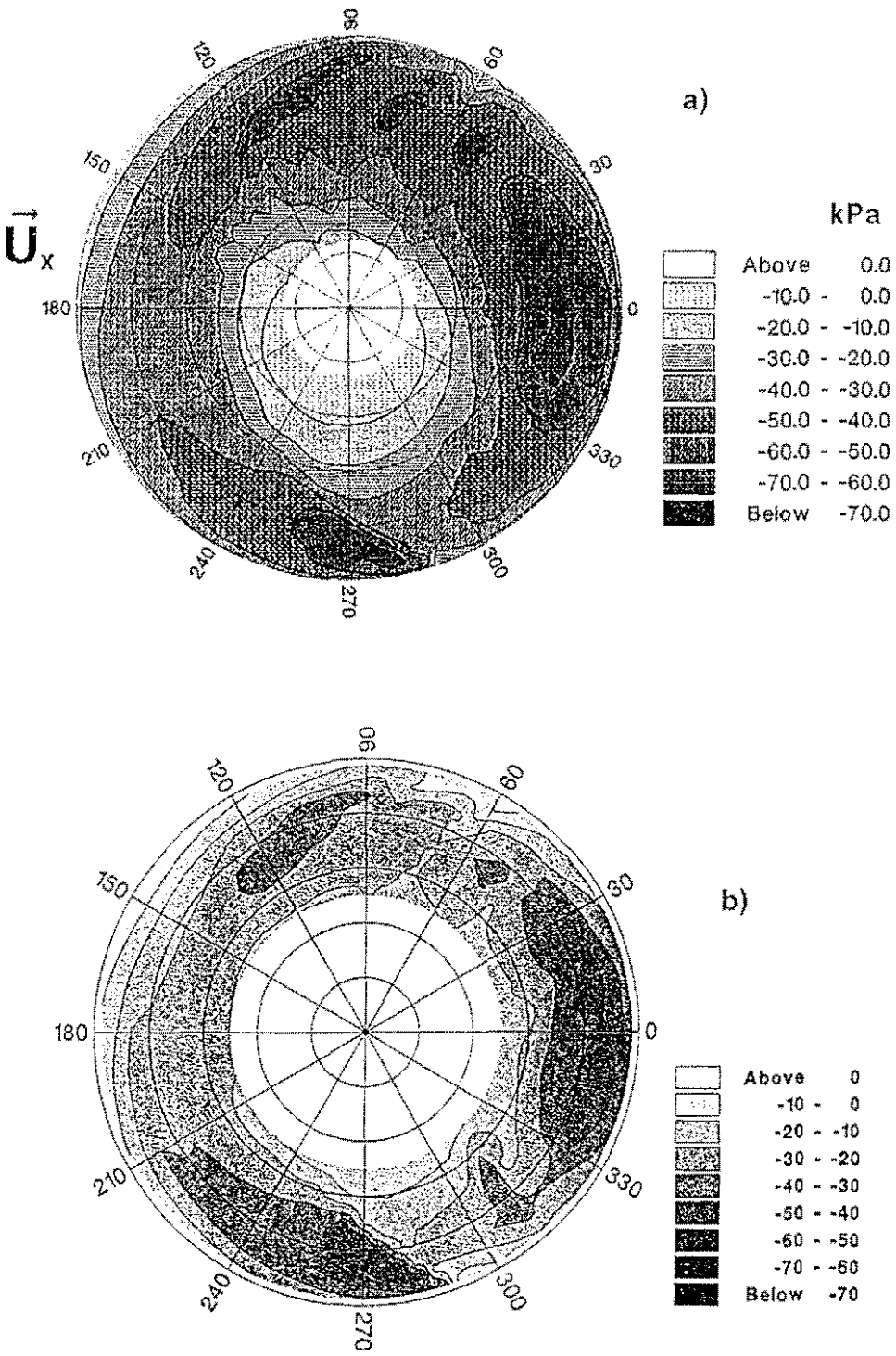

Fig. 16: Contour plot on the rotor disk of the computed (a) and the measured (b) differential pressures for the radial position x/c = 0.03

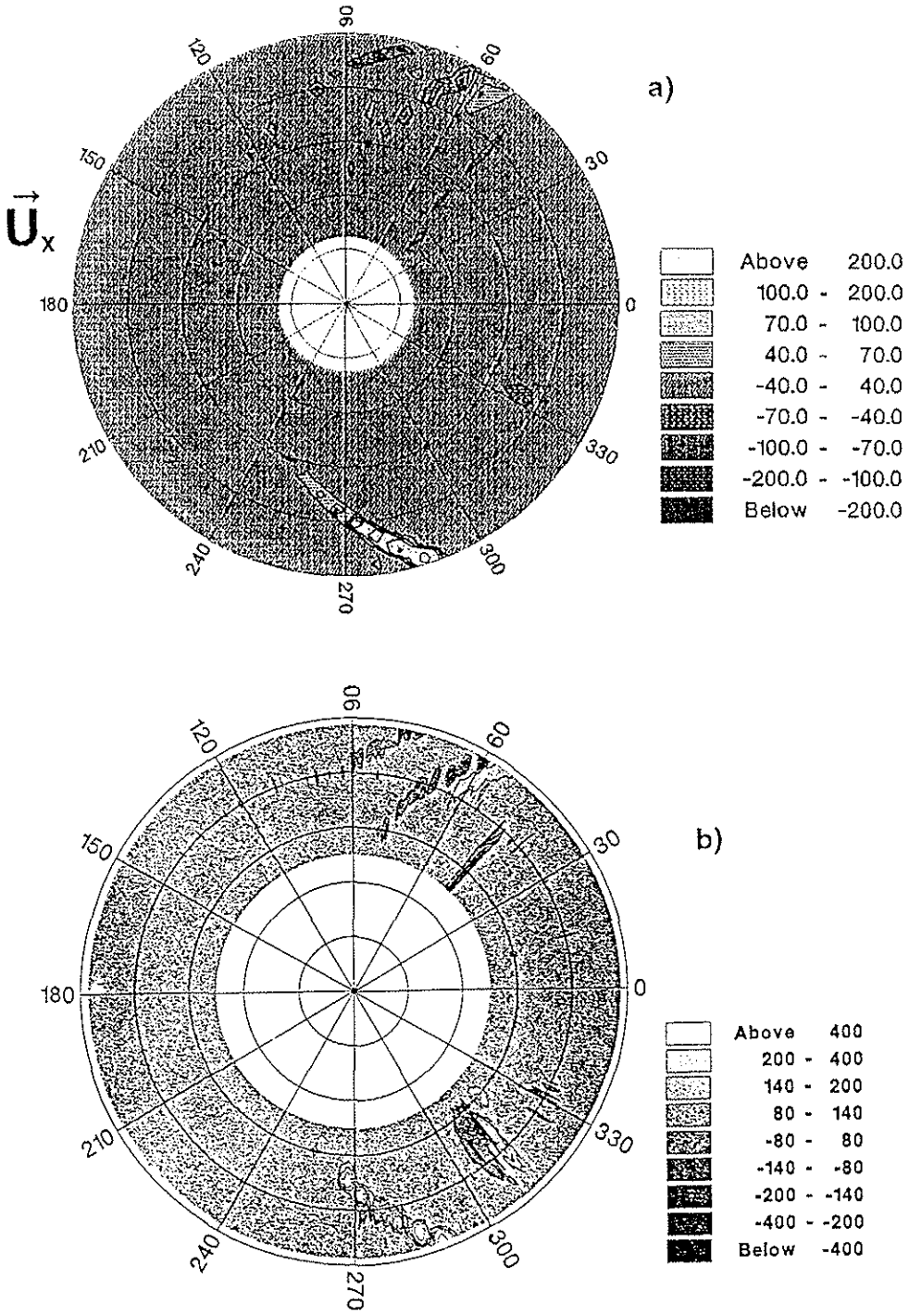

Fig. 17: Contour plot on the rotor disk of the time derivative of the computed (a) and the measured (b) differential pressures for x/c = 0.03